Exclusive CX_3CR1 dependence of kidney DCs impacts glomerulonephritis progression

Katharina Hochheiser,[1] Christoph Heuser,[1] Torsten A. Krause,[1] Simon Teteris,[1] Anissa Ilias,[2] Christina Weisheit,[3] Florian Hoss,[1] André P. Tittel,[1] Percy A. Knolle,[1,4] Ulf Panzer,[5] Daniel R. Engel,[1] Pierre-Louis Tharaux,[2] and Christian Kurts[1]

[1]Institutes of Molecular Medicine and Experimental Immunology, Rheinische Friedrich-Wilhelms University, Bonn, Germany.
[2]Paris Cardiovascular Research Centre, INSERM, and Université Paris Descartes, Sorbonne Paris Cité, Paris, France.
[3]Department of Anesthesiology and Intensive Care Medicine, Rheinische Friedrich-Wilhelms University, Bonn, Germany.
[4]Institute of Molecular Immunology, Technische Universität, Munich, Germany.
[5]III Medizinische Klinik, Universitätsklinikum Hamburg-Eppendorf, Germany.

DCs and macrophages both express the chemokine receptor CX_3CR1. Here we demonstrate that its ligand, CX_3CL1, is highly expressed in the murine kidney and intestine. CX_3CR1 deficiency markedly reduced DC numbers in the healthy and inflamed kidney cortex, and to a lesser degree in the kidney medulla and intestine, but not in other organs. CX_3CR1 also promoted influx of DC precursors in crescentic glomerulonephritis, a DC-dependent aggressive type of nephritis. Disease severity was strongly attenuated in CX_3CR1-deficient mice. Primarily CX_3CR1-dependent DCs in the kidney cortex processed antigen for the intrarenal stimulation of T helper cells, a function important for glomerulonephritis progression. In contrast, medullary DCs played a specialized role in inducing innate immunity against bacterial pyelonephritis by recruiting neutrophils through rapid chemokine production. CX_3CR1 deficiency had little effect on the immune defense against pyelonephritis, as medullary DCs were less CX_3CR1 dependent than cortical DCs and because recruited neutrophils produced chemokines to compensate for the DC paucity. These findings demonstrate that cortical and medullary DCs play specialized roles in their respective kidney compartments. We identify CX_3CR1 as a potential therapeutic target in glomerulonephritis that may involve fewer adverse side effects, such as impaired anti-infectious defense or compromised DC functions in other organs.

Introduction

DCs exist in virtually all organs. They gather antigens and activate T cells after migrating into the draining lymph nodes. Additionally, tissue-resident DCs modulate local immune responses by regulating infiltrating effector cells or memory T cells (1–4). Tissue macrophages (MPs) differ from DCs by a higher capacity to endocytose and degrade antigen and to clear pathogens and apoptotic cells and by a lower ability to activate T cells (5). The classification of APCs as DCs or MPs is still controversial. The demarcation between MP and DC functions is not absolute, and cells with combined functionality in varying degrees exist (5). We recently demonstrated that kidney cells expressing CD11c and MHC-II possessed DC, but not MP, functionality (6). A recent transcriptome analysis of $CD11c^+$ kidney cells supported this classification (7).

In the healthy kidney, DCs form an extensive network in the tubulointerstitium (8) that maintains tissue homeostasis and serves sentinel functions against various forms of injury (9, 10). They play a sentinel role in pyelonephritis (PN), the most common renal infection, in which uropathogenic *E. coli* ascend from the bladder through the tubular system into the kidney (4). In nephrotoxic nephritis (NTN), a murine model of human crescentic glomerulonephritis (GN) (11), kidney DCs initially performed an antiinflammatory function by attracting regulatory NKT cells (3, 12) but matured when inflammation became chronic (13). Then, they produced chemokines and cytokines that attracted and stimulated Th1 and Th17 cells, resulting in a mononuclear tubulointerstitial infiltrate that drove disease progression through an intrarenal delayed-type hypersensitivity (DTH) response (2, 14).

Chemokines play important roles in the tissue recruitment of leukocytes, both in homeostasis and inflammation. Distinct chemokine receptors have been linked with specific immune cells, the type of immune responses, and immune cell recruitment into particular organs. Thus, CCR9 is associated with immune cells in the intestine (15), CCR4 is associated with those in the skin and lung (16, 17), and CCR6 regulates the entry of Th17 cells and Tregs into the brain (18, 19). A specific receptor for the kidney has not yet been identified.

The chemokine receptor CX_3CR1, also known as the fractalkine receptor, is expressed by monocytes, DCs, and MPs and on some memory T cells. CX_3CR1 reporter mice, in which GFP expression is driven by the CX_3CR1 promoter (20), have greatly facilitated analysis of these cells. However, mice lacking this receptor showed few abnormalities in the steady state, such as a reduced glucose tolerance due to CX_3CR1 expression on pancreatic islet β cells (21) or lower MP numbers in the intestinal lamina propria (22). Intestinal DCs required CX_3CR1 to sample antigen from the intestinal lumen (23). Little is known about the role of CX_3CR1 in tissue DC homeostasis, especially in the kidney.

CX_3CR1 has one ligand, CX_3CL1, which is expressed by various tissue cells. A recent study using CX_3CL1 reporter mice demonstrated remarkably strong expression of CX_3CL1 in kidney glomerular and tubular cells (24). That study focused on intestinal DCs and therefore addressed neither the exact identity of CX_3CL1^+ kidney cells, nor functional implications. In the human system, CX_3CL1 has been detected on tubular epithelial cells, especially under inflammatory conditions, like acute allograft rejection and

Conflict of interest: The authors have declared that no conflict of interest exists.
Citation for this article: *J Clin Invest.* 2013;123(10):4242–4254. doi:10.1172/JCI70143.

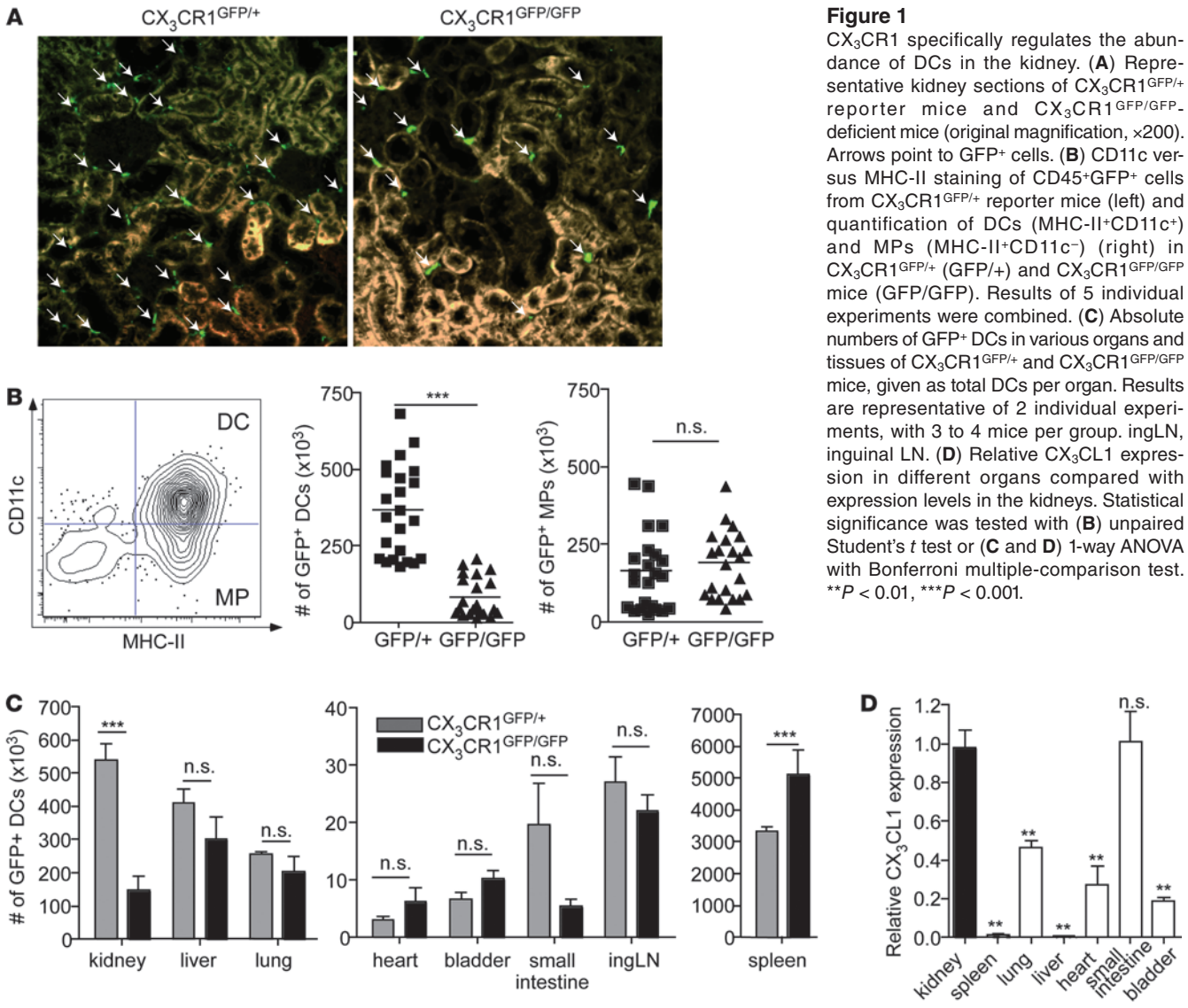

Figure 1

CX_3CR1 specifically regulates the abundance of DCs in the kidney. (**A**) Representative kidney sections of $CX_3CR1^{GFP/+}$ reporter mice and $CX_3CR1^{GFP/GFP}$-deficient mice (original magnification, ×200). Arrows point to GFP^+ cells. (**B**) CD11c versus MHC-II staining of $CD45^+GFP^+$ cells from $CX_3CR1^{GFP/+}$ reporter mice (left) and quantification of DCs ($MHC\text{-}II^+CD11c^+$) and MPs ($MHC\text{-}II^+CD11c^-$) (right) in $CX_3CR1^{GFP/+}$ (GFP/+) and $CX_3CR1^{GFP/GFP}$ mice (GFP/GFP). Results of 5 individual experiments were combined. (**C**) Absolute numbers of GFP^+ DCs in various organs and tissues of $CX_3CR1^{GFP/+}$ and $CX_3CR1^{GFP/GFP}$ mice, given as total DCs per organ. Results are representative of 2 individual experiments, with 3 to 4 mice per group. ingLN, inguinal LN. (**D**) Relative CX_3CL1 expression in different organs compared with expression levels in the kidneys. Statistical significance was tested with (**B**) unpaired Student's *t* test or (**C** and **D**) 1-way ANOVA with Bonferroni multiple-comparison test. $^{**}P < 0.01$, $^{***}P < 0.001$.

GN (25). Concomitantly, an infiltration of CX_3CR1^+ monocytes and T cells into inflamed kidneys was observed in patients (26, 27).

Preclinical studies in disease models showed both beneficial and adverse effects of CX_3CR1 in a context-dependent manner. Thus, CX_3CR1 aggravated heart transplant rejection (28) and arteriosclerosis by recruiting monocytes and promoting their survival (29, 30). Conversely, CX_3CR1 also enhanced monocyte survival in liver injury, but this attenuated hepatitis (31). Other protective roles of CX_3CR1 include preventing subretinal accumulation of microglia in degenerative macular eye disease (32) and monocyte recruitment to the spleen in listeriosis (33). In kidney ischemia/reperfusion and hypertensive kidney fibrosis, CX_3CR1 contributed to monocyte recruitment (34) and aggravated fibrosis (35, 36). Conflicting studies exist on the role of CX_3CR1 in GN. While antibody blockade of CX_3CR1 reduced monocyte and $CD8^+$ T cell infiltration and ameliorated disease in rats (37), immune complex GN in CD1 mice was unaltered in CX_3CR1-deficient mice (28). The role of CX_3CR1 in NTN is presently unclear.

The kidney can be macroscopically divided into 2 compartments, the cortex and the medulla, which harbor different parts of the nephrons. The glomeruli and the proximal tubuli are found in the cortex, and the descending loop of Henle enters the medulla, returns to the cortex, and continues as the distal tubule, which enters the collecting tubules that again descend into the medulla. DCs are located in both compartments, but due to differential blood supply and osmotic concentrations they encounter highly differential environmental conditions. There is no information about functional differences between cortical and medullary DCs.

Here, we hypothesized that cortical DCs might be critical in GN, as the glomeruli are located in the cortex, whereas medullary DCs might be more important in PN, because the ascending bacteria first pass through the medulla. Our present findings confirm this hypothesis and demonstrate that CX_3CR1 preferentially affects cortical DCs, identifying new therapeutic opportunities in GN.

Results

Dependence of kidney DCs and MPs on CX_3CR1 in healthy mice. CX_3CR1 is abundantly expressed on most kidney APCs, whereas other immune cells constituted only minor fractions among

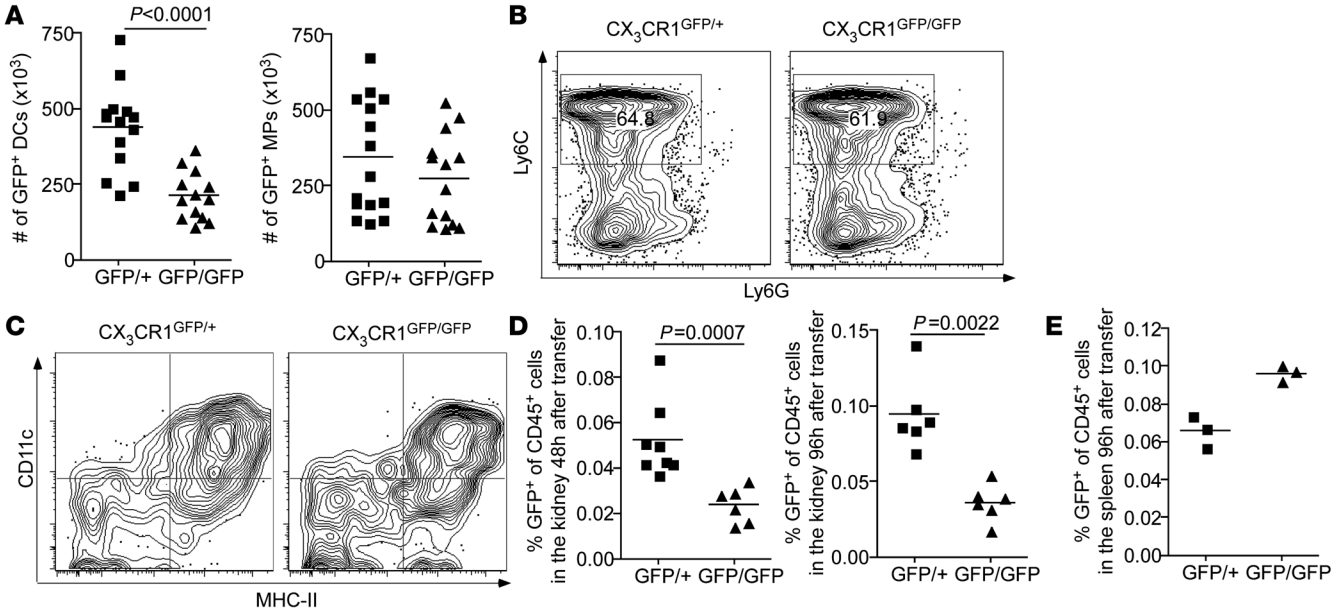

Figure 2

Dependence of kidney DCs and MPs on CX_3CR1 in NTN. (**A**) Absolute numbers of GFP^+ DCs and MPs per kidney in $CX_3CR1^{GFP/+}$ and $CX_3CR1^{GFP/GFP}$ mice on day 10 after NTN induction. Results are combined from 4 individual experiments. (**B**) Ly6C expression on GFP^+ bone marrow cells from $CX_3CR1^{GFP/+}$ and $CX_3CR1^{GFP/GFP}$ mice before transfer into nephritic WT mice. (**C**) Representative FACS plots of CD11c and MHC-II expression on GFP^+ cells recovered from kidneys of nephritic WT mice, which had received 10^6 GFP^+ bone marrow cells from $CX_3CR1^{GFP/+}$ or $CX_3CR1^{GFP/GFP}$ mice 96 hours before. (**D**) Proportion of GFP^+ cells among $CD45^+$ cells in the kidneys of nephritic WT mice 48 and 96 hours after transfer of 10^6 GFP^+ bone marrow cells from $CX_3CR1^{GFP/+}$ or $CX_3CR1^{GFP/GFP}$ mice. (**E**) Proportion of GFP^+ cells among $CD45^+$ cells in the spleens of nephritic WT mice 96 hours after transfer of 10^6 GFP^+ bone marrow cells from $CX_3CR1^{GFP/+}$ or $CX_3CR1^{GFP/GFP}$ mice. Data points represent (**A** and **E**) individual mice or (**D**) organs. Results are representative 2 individual experiments, with 3 to 4 mice per group. Statistical significance was tested with (**A**) the unpaired Student's *t* test or (**D**) the 2-tailed Mann-Whitney test.

CX_3CR1^+ kidney cells (ref. 8 and Supplemental Figure 1, A–C; supplemental material available online with this article; doi:10.1172/JCI70143DS1). The functional role of CX_3CR1 in kidney APCs is unclear. When we compared kidney sections of $CX_3CR1^{GFP/+}$ mice (expressing a GFP reporter in CX_3CR1^+ cells) and of $CX_3CR1^{GFP/GFP}$ mice (expressing the GFP reporter and deficient for CX_3CR1) by fluorescence microscopy, an obvious reduction of GFP^+ cells in the absence of CX_3CR1 was noted (Figure 1A). Analysis of kidney single cell suspensions by flow cytometry (gating strategy shown in Supplemental Figure 1D) revealed that exclusively the CX_3CR1^+ APCs expressing CD11c, which have been shown to possess DC functionality (6), were reduced by 75% in $CX_3CR1^{GFP/GFP}$ mice, whereas $CD11c^-$ MPs were slightly, albeit not statistically significantly, enhanced (Figure 1B). Total DC and MP numbers did not differ between WT and $CX_3CR1^{GFP/+}$ mice (Supplemental Figure 2A), indicating that the latter could serve as CX_3CR1-competent controls.

To study whether the reduction in DC numbers was unique to the kidney, we compared their abundance in different tissues from $CX_3CR1^{GFP/+}$ and $CX_3CR1^{GFP/GFP}$ mice. There was no reduction in liver, lung, heart, bladder, lymph nodes, or spleen (Figure 1C). DCs were less frequent in CX_3CR1-deficient mice in the small intestine, but their absolute numbers were more than an order of magnitude lower than in 1 kidney (Figure 1C). The spleens of $CX_3CR1^{GFP/GFP}$ mice contained approximately 40% more GFP^+ DCs than those of $CX_3CR1^{GFP/+}$ controls (Figure 1C), which might be explained by different homing of DC precursors.

$CD11c^-$ GFP^+ MPs were substantially reduced in the intestines of CX_3CR1-deficient mice (Supplemental Figure 2B), consistent with a recent report (22). There was no reduction of $CD11c^-$ GFP^+ cells in kidney, liver, lung, heart, bladder, dermis, epidermis, bone marrow, spleen, and brain (Supplemental Figure 2C).

We speculated that the particularly strong CX_3CR1 dependence of DCs in the kidney might be due to high expression of its ligand, CX_3CL1, in this organ. Indeed, when we determined CX_3CL1 by quantitative RT-PCR, its expression in the kidney was much higher than that in other organs except the small intestine (Figure 1D), providing a plausible explanation as to why DCs depended on CX_3CR1 only in these organs (Figure 1C). There were no differences in CX_3CL1 expression between CX_3CR1-deficient and competent mice (Supplemental Figure 2D), ruling out feedback regulation of ligand expression by the receptor.

Dependence of kidney DCs and MPs on CX_3CR1 in NTN. To study whether kidney DCs depended on CX_3CR1 also under inflammatory conditions, we induced NTN, a widely studied model for crescentic GN. Ten days after disease induction, GFP^+ DCs were scarcer in the kidneys of $CX_3CR1^{GFP/GFP}$ mice compared with $CX_3CR1^{GFP/+}$ mice (Figure 2A). Of note, there was also a slight, albeit not statistically significant, reduction of renal GFP^+ MP numbers at that time point (Figure 2A). The small numbers of CX_3CR1^+ non-APCs, such as T cells, NK cells, and mast cells, differed very little between $CX_3CR1^{GFP/+}$ and $CX_3CR1^{GFP/GFP}$ mice, both under homeostatic conditions and in NTN (Supplemental Figure 1, A and B).

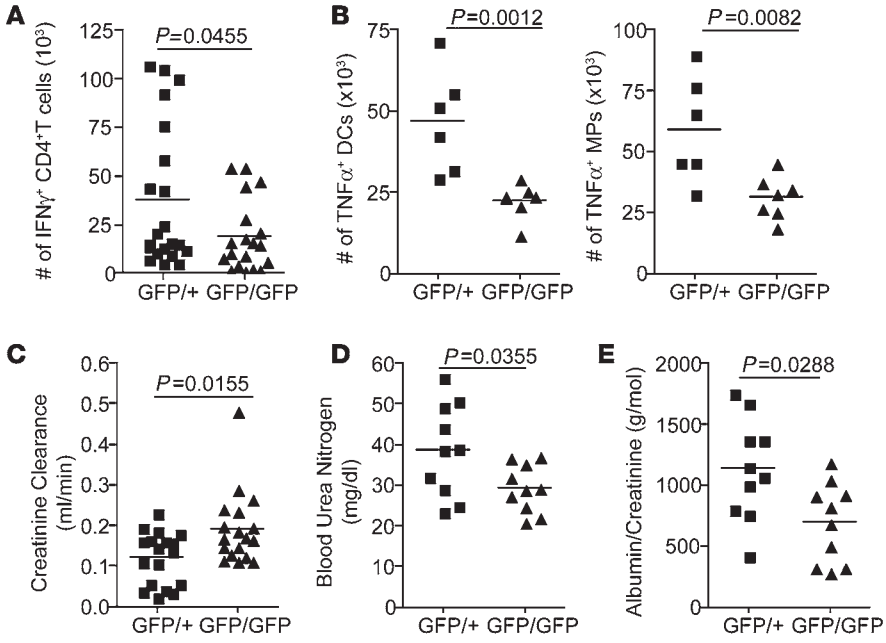

Figure 3
CX_3CR1 deficiency reduces intrarenal Th1 response and improves kidney function. (**A**) Absolute numbers of IFN-γ–producing $CD4^+$ T cells and (**B**) of TNF-producing DCs and MPs per kidney of $CX_3CR1^{GFP/+}$ reporter mice and $CX_3CR1^{GFP/GFP}$-deficient mice 10 days after NTN induction, as determined by intracellular flow cytometry. In **A**, cell numbers in 4 individual experiments were given as percentage of the mean cell number in the CX_3CR1-competent groups. (**C**) Creatinine clearance in $CX_3CR1^{GFP/+}$ and $CX_3CR1^{GFP/GFP}$ mice 10 days after NTN induction. (**D**) Blood urea nitrogen in $CX_3CR1^{+/+}$ and $CX_3CR1^{GFP/GFP}$ mice 10 days after NTN induction. (**E**) Albumin excretion normalized to creatinine by $CX_3CR1^{GFP/+}$ and $CX_3CR1^{GFP/GFP}$ mice 10 days after NTN induction. Urine was collected for 12 hours. Data points represent individual mice, and results (**A**–**C**) are combined from 2 to 4 individual experiments, with 2 to 5 mice per group, or (**D** and **E**) are representative of 2 individual experiments, with 10 mice per group. Statistical significance was tested with the 2-tailed Mann-Whitney test.

We next asked whether the reduction of kidney DCs in nephritic $CX_3CR1^{GFP/GFP}$ mice was only a consequence of the reduced DC numbers under homeostatic conditions (Figure 1B) or whether the recruitment of DC precursors under inflammatory conditions also depended on CX_3CR1. We addressed this question by adoptively transferring 10^6 GFP^+ bone marrow cells from $CX_3CR1^{GFP/+}$ and $CX_3CR1^{GFP/GFP}$ mice into WT mice 1 day after NTN induction. More than 60% of the GFP^+ bone marrow cells expressed Ly6C, which is characteristic of inflammatory monocytes (Figure 2B). Influx of GFP^+ cells into the kidneys was analyzed 2 and 4 days after transfer. GFP^+ cells expressing the DC markers CD11c and MHC-II were detected in inflamed kidneys (Figure 2C). Importantly, far fewer CX_3CR1-deficient cells entered nephritic kidneys at both time points (Figure 2D), whereas more of them were recovered from the spleens (Figure 2E). This indicates that CX_3CR1 contributes to entry of DC precursors into the inflamed kidney. In the absence of CX_3CR1, these cells relocated to the spleen, similar to our observations in healthy mice (Figure 1C). We did not detect the marker Ly6C on immigrated DCs (data not shown). This may be due to the rapid loss of this marker soon after tissue entry of $Ly6C^+$ monocytes, as recently shown in the lung (38).

CX_3CR1 deficiency attenuates NTN. We recently showed that kidney DC maturation stimulates the intrarenal DTH that drives NTN (13). The dearth of DCs in nephritic $CX_3CR1^{GFP/GFP}$ mice suggested that DTH should be reduced in these mice. Indeed, flow cytometric analysis of kidney single cell suspensions (gating strategies shown in Supplemental Figure 1, D–F) on day 10 after disease induction revealed reduced numbers of IFN-γ^+ $CD4^+$ T cells (Figure 3A) and of TNF-producing DCs and MPs in CX_3CR1-deficient mice (Figure 3B), suggesting an attenuated intrarenal DTH response. IL-17^+ $CD4^+$ T cells were only slightly and not significantly reduced (Supplemental Figure 3B), consistent with the recent finding that Th17 cells are more important in the early disease phase (14). Other early immune mediators were also not affected by CX_3CR1 deficiency, as evidenced by unchanged IFN-γ, TNF, CXCL10, and CXCL16 expression in $CX_3CR1^{GFP/+}$ and $CX_3CR1^{GFP/GFP}$ mice after 24 hours (Supplemental Figure 3A).

Functional parameters like creatinine clearance, blood urea nitrogen, and proteinuria were improved in $CX_3CR1^{GFP/GFP}$ mice (Figure 3, C–E), and histological examination of kidney sections revealed fewer tubular casts and crescents in $CX_3CR1^{GFP/GFP}$ mice on day 10 (Supplemental Figure 3C), indicating that the loss of CX_3CR1 attenuates NTN. On day 15, the histological features of kidney damage were even more pronounced (Figure 4, A–C). $CX_3CR1^{GFP/GFP}$ mice also featured fewer periglomerular $F4/80^+$ cells (Figure 4, D and E), indicating a reduction in DCs and/or MPs. Despite their reduced numbers (Figure 2A), kidney DCs of $CX_3CR1^{GFP/GFP}$ mice still formed periglomerular infiltrates (6) in NTN (Figure 4F), indicating that CX_3CR1 was dispensable for intrarenal APC migration toward inflamed glomeruli.

Cell-intrinsic DC functions are independent of CX_3CR1 expression. To understand how CX_3CR1 deficiency attenuated intrarenal DTH and nephritis symptoms, we asked whether DCs were functionally defective in the absence of this receptor. We first examined the systemic Th1 response against sheep Ig, which is induced by DCs in lymphatic tissues after injection of the nephrotoxic sheep serum (39). This response was unaltered, as evidenced by similar subcutaneous DTH response against sheep Ig (Figure 5A) and by similar production of the Th1 and Th17 cytokines, IFN-γ, TNF, and IL-17, by splenocytes (Figure 5B). These findings excluded the possibility that the attenuated intrarenal DTH response in $CX_3CR1^{GFP/GFP}$ mice resulted from a failure to activate a nephritogenic T cell response.

We therefore focused on intrarenal DCs. CX_3CR1-deficient and -competent kidney DCs from nephritic mice expressed equal levels of costimulatory molecules and MHC-II (Figure 5C). Next, we studied their ability to capture antigen by injecting the model antigen, OVA, a 45-kDa protein that can constitutively pass the glomerular filter (40). Regardless of CX_3CR1 expression, DCs took up similar amounts of OVA (Figure 5D). To examine the principal DC function, the activation of naive T cells, we injected CX_3CR1-deficient and CX_3CR1-competent nephritic mice with OVA and cocultured kidney DCs with OVA-specific Th cells (OT-II cells). $CX_3CR1^{GFP/+}$ and $CX_3CR1^{GFP/GFP}$ DCs elicited similar

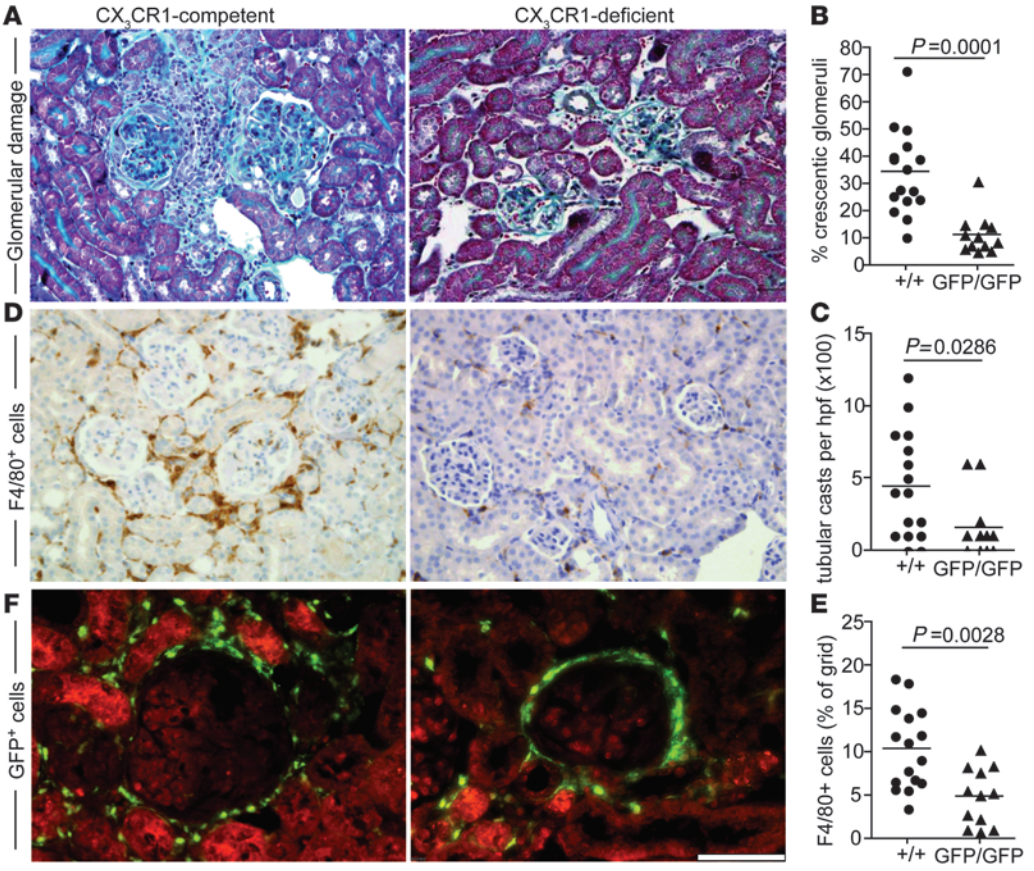

Figure 4
CX_3CR1 deficiency attenuates NTN. (**A**) Kidney sections of $CX_3CR1^{+/+}$ and $CX_3CR1^{GFP/GFP}$ animals 15 days after NTS challenge (Masson trichrome; original magnification, ×200). (**B**) Percentage of crescentic glomeruli in histological sections of $CX_3CR1^{+/+}$ and $CX_3CR1^{GFP/GFP}$ mice on day 15 after disease induction. (**C**) Tubular casts per high-power field (hpf) (original magnification, ×100) in $CX_3CR1^{+/+}$ and $CX_3CR1^{GFP/GFP}$ mice 15 days after NTS challenge. (**D**) Representative microphotographs of immunostained F4/80+ cells in kidney cortices from $CX_3CR1^{+/+}$ and $CX_3CR1^{GFP/GFP}$ mice on day 15 after NTN induction (original magnification, ×200). (**E**) Quantification of infiltrating F4/80+ cells in $CX_3CR1^{+/+}$ and $CX_3CR1^{GFP/GFP}$ animals 15 days after NTS challenge. (**F**) Immunofluorescence microscopy of kidney sections from nephritic $CX_3CR1^{GFP/+}$ and $CX_3CR1^{GFP/GFP}$ mice on day 10 after NTN induction (red [autofluorescence], green [GFP]). Scale bar: 50 μm. Data points represent individual mice, and (**D**–**F**) results are representative of 2 individual experiments, with 12 to 16 mice per group. Statistical significance was tested by 2-tailed Mann-Whitney test.

proliferation profiles and cytokine production by OT-II cells (Figure 5, E and F). Therefore, the observed differences in disease severity were not due to DC-intrinsic functional defects, supporting their reduced numbers as an underlying reason.

DCs in the renal cortex are especially dependent on CX3CR1. When we reexamined kidney sections of healthy $CX_3CR1^{GFP/+}$ and $CX_3CR1^{GFP/GFP}$ mice by immunofluorescence microscopy, the paucity of GFP+ cells in the latter mice seemed to preferentially affect the kidney cortex (Figure 6A). To verify this histological impression in a quantitative manner and to distinguish between DCs and MPs, we surgically separated the renal medulla from the cortex, produced single cell suspensions by separate collagen digestion, and analyzed these by flow cytometry. The cortex of $CX_3CR1^{GFP/+}$ mice contained 3 times more GFP+ cells than the medulla, and 80% of them expressed the DC marker CD11c, whereas less than 40% of GFP+ cells in the medulla did so (Figure 6, B and C). Consequently, the absolute numbers of GFP+ DCs were about 6 times higher in the cortex than in the medulla (Figure 6D). In $CX_3CR1^{GFP/GFP}$ mice, DC numbers were reduced 9 fold from 200×10^3 to 22×10^3 cells per kidney cortex, whereas medullary DCs were reduced 3.5 fold from 38×10^3 to 11×10^3 cells per kidney (Figure 6D). MP numbers were increased 2.5 fold in the cortices of $CX_3CR1^{GFP/GFP}$ mice (Figure 6E). Of note, the mice used in this experiment were younger than those used in the other experiments (Figure 1 and Figure 6, G and H), explaining the relatively low absolute DC numbers. Nevertheless, DC numbers were similarly reduced, indicating that the kidney DC deficiency in CX_3CR1-deficient mice was age independent.

The kidney cortices of nephritic $CX_3CR1^{GFP/+}$ mice contained 416×10^3 GFP+ DCs, compared with 164×10^3 DCs in $CX_3CR1^{GFP/GFP}$ mice (60% reduction), whereas only 96×10^3 DCs were seen in the medullas of CX_3CR1-competent mice and 44×10^3 DCs were seen in those of CX_3CR1-deficient mice (55% reduction) (Figure 6F). Thus, even though proportional DC reduction was similar, the absolute deficit of kidney DCs in nephritis was more prominent in the cortex (–252×10^3 DCs) than in the medulla (–52×10^3 DCs). Furthermore, there were approximately 32×10^3 fewer MPs in the cortices and approximately 20×10^3 fewer medullary MPs in CX_3CR1-deficient nephritic

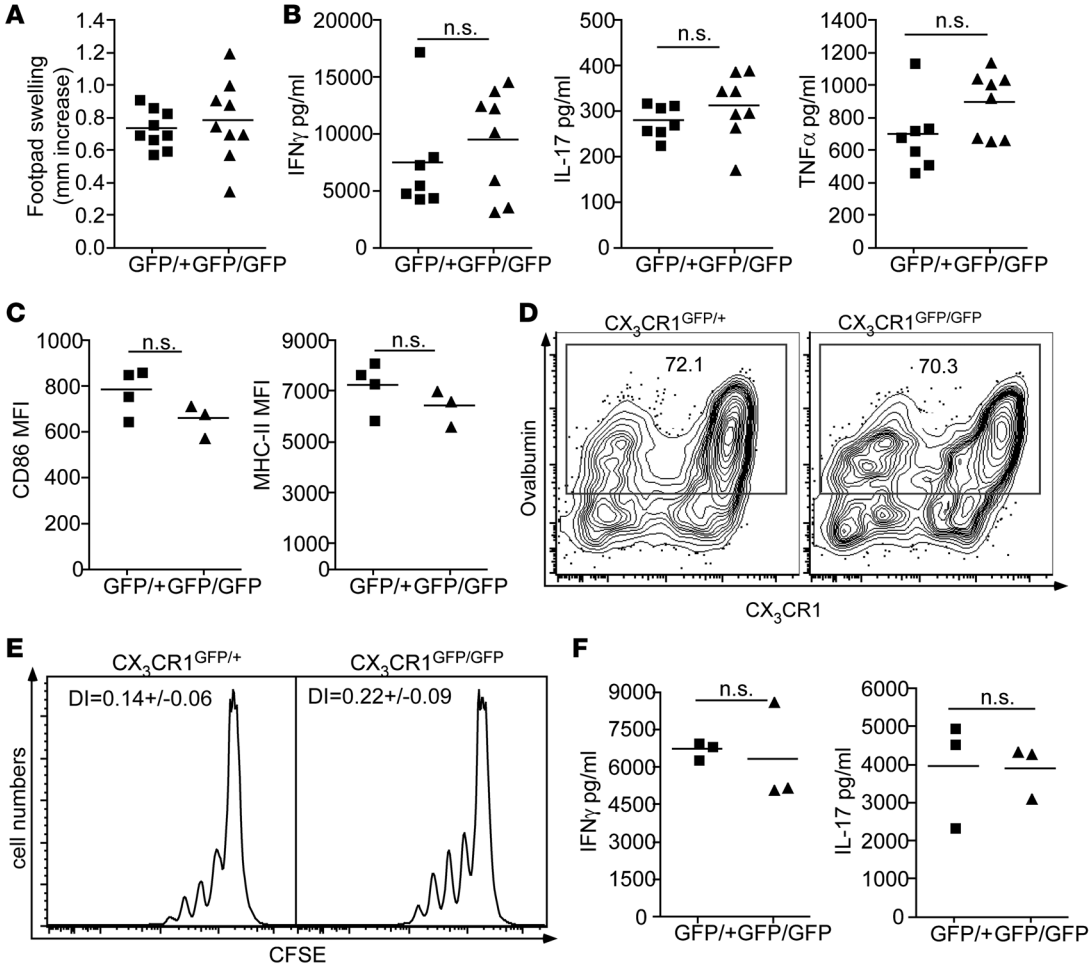

Figure 5

Cell-intrinsic DC functions are unaltered by CX_3CR1 deficiency. (**A**) DTH reaction in the skin of $CX_3CR1^{GFP/+}$ reporter mice and $CX_3CR1^{GFP/GFP}$-deficient mice, rechallenged by footpad injection with NTS. Depicted is footpad swelling in comparison with the contralateral footpad injected with vehicle control. (**B**) IFN-γ, IL-17, and TNF concentration in the supernatant of 24-hour splenocyte culture from nephritic $CX_3CR1^{GFP/+}$ and $CX_3CR1^{GFP/GFP}$ mice rechallenged with NTS. 10^7 total splenocytes were cultured for 24 hours in 1 ml medium and 1:200 NTS. (**C**) MFI of CD86 and MHC-II expression on kidney DCs from $CX_3CR1^{GFP/+}$ mice and $CX_3CR1^{GFP/GFP}$ mice, determined by flow cytometry. (**D**) Representative FACS plots of the in vivo uptake of fluorescently labeled OVA by kidney DCs of nephritic $CX_3CR1^{GFP/+}$ and $CX_3CR1^{GFP/GFP}$ mice gated on $CD45^+MHC\text{-}II^+CD11c^+$ cells. Numbers show percentages of OVA^+ DCs. (**E**) Representative histograms of T cell proliferation and CFSE dilution and division indices (DI) in a coculture of OVA-specific T cells and kidney DCs from nephritic $CX_3CR1^{GFP/+}$ and $CX_3CR1^{GFP/GFP}$ mice injected with 1 mg OVA 1 hour prior to cull. (**F**) IFN-γ and IL-17 concentrations in supernatants of 72-hour cocultures from **E**. Data points represent individual mice, and results are representative of 2 to 4 experiments, with 3 to 4 mice per group. Statistical significance was tested with the unpaired Student's *t* test.

mice (Figure 6G). Taken together, our findings demonstrated that, under homeostatic conditions, CX_3CR1 primarily affected DCs in the cortex, and, in the condition of nephritis, affected both cortical and medullary DCs and to a lesser extend also MPs.

Cortical, but not medullary, DCs can stimulate Th cells in GN. We reasoned that the proximity of cortical DCs to the glomeruli might render these cells particularly relevant in GN. When we compared the phenotype of medullary and cortical APCs in healthy mice, we observed similar expression of CD11b, F4/80, and CX_3CR1 and higher CD11c expression on cortical CX_3CR1^+ cells (Figure 7A). For the most part, cortical and medullary DCs expressed similar levels of MHC-II and of the costimulatory molecules CD80, CD86, and CD40 under homeostatic conditions (Figure 7B), notwithstanding some variability of expression levels between experiments. In nephritic mice, expression of CD40 and MHC-II on cortical DCs slightly exceeded that on medullary DCs in 3 out of 5 experiments, consistent with higher maturation of the former (Figure 7B).

NTN is driven by a Th cell–dependent intrarenal DTH (11). Therefore, we cocultured cortical and medullary DCs with the model antigen, OVA, and OT-II cells. OVA-loaded cortical and medullary DCs from healthy mice caused little T cell proliferation compared with control splenic DCs (Figure 7C). By contrast, OVA-loaded DCs from the cortices of nephritic mice induced strong OT-II cell proliferation (Figure 7, C and D) and secretion of IFN-γ and IL-17 (Figure 7E). Remarkably, medullary DCs from nephritic kidneys still only elicited minimal OT-II cell proliferation and cytokine production (Figure 7, C–E). These results suggested that Th cell stimulation during NTN depends mainly on cortical DCs, implying that only these DCs drive NTN progression.

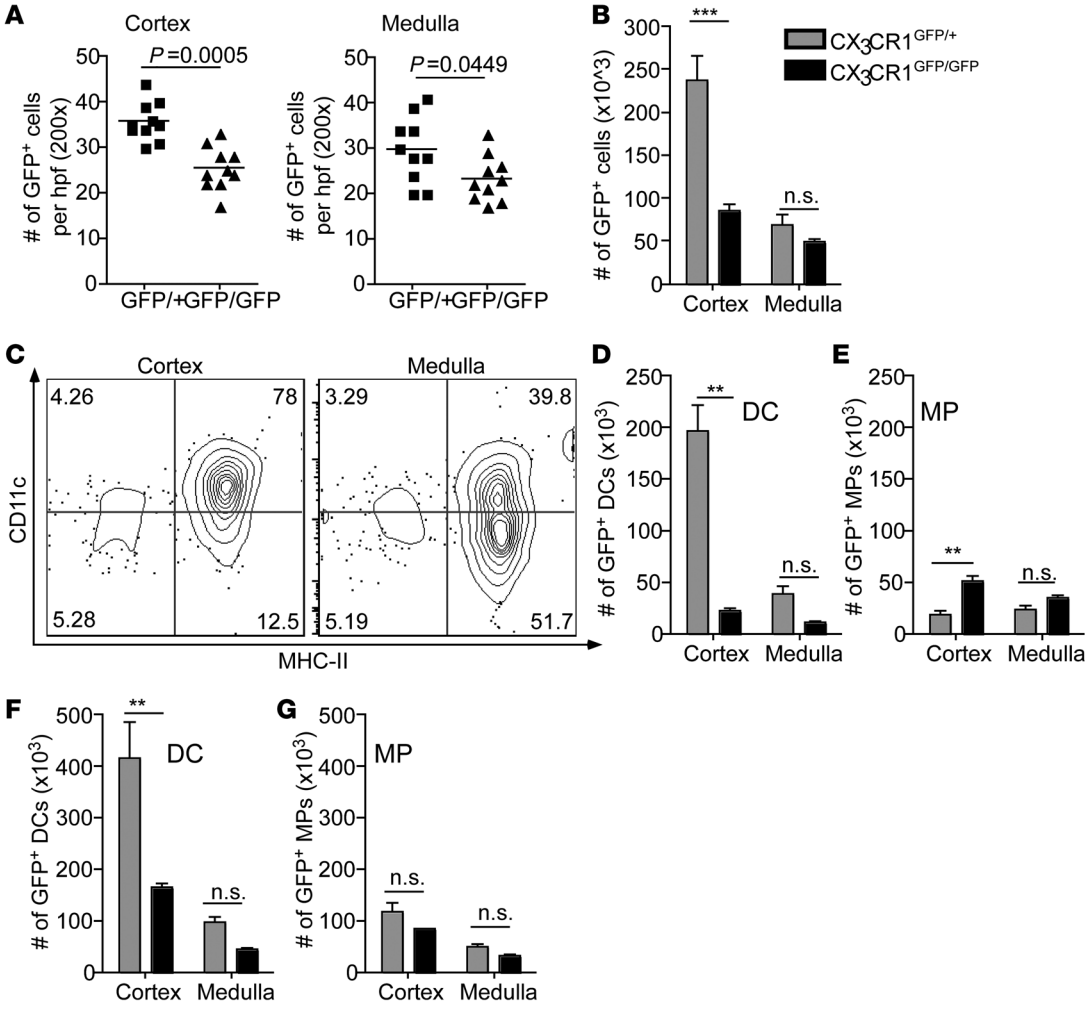

Figure 6

DCs in the renal cortex particularly depend on CX_3CR1. (**A**) Histological quantification of GFP^+ cells in cortical and medullary kidney sections of healthy $CX_3CR1^{GFP/+}$ reporter mice and $CX_3CR1^{GFP/GFP}$-deficient mice. Each data point represents 1 high-power field (original magnification, ×200). Statistical significance was calculated by Mann Whitney test. (**B**) Absolute numbers of GFP^+ cells in the cortices and medullas of 1 kidney of healthy $CX_3CR1^{GFP/+}$ mice (gray bars) and $CX_3CR1^{GFP/GFP}$ mice (black bars), determined by flow cytometry. (**C**) Representative FACS plots of $CD45^+GFP^+$ cells in kidney cortices and medullas of $CX_3CR1^{GFP/+}$ mice. (**D** and **E**) Absolute numbers of (**D**) DCs and (**E**) MPs in the renal cortices and medullas of healthy $CX_3CR1^{GFP/+}$ mice (gray bars) and $CX_3CR1^{GFP/GFP}$ mice (black bars). (**F** and **G**) Absolute numbers of (**F**) DCs and (**G**) MPs in the cortices and the medullas of 1 kidney of nephritic $CX_3CR1^{GFP/+}$ mice (gray bars) and $CX_3CR1^{GFP/GFP}$ mice (black bars) on day 10 after NTN induction. Results are representative of 2 to 3 individual experiments, with 3 to 4 mice per group. Statistical analysis was performed using 1-way ANOVA with Bonferroni multiple-comparison. $^{**}P < 0.01$, $^{***}P < 0.001$.

Medullary DCs poorly process antigen for MHC-II presentation. To understand why medullary DCs poorly stimulated Th cells, we first examined their survival in vitro. A similar fraction of cortical and medullary DCs survived a culture period of 24 hours (cortical DCs: 55.4% ± 0.7% survival; medullary DCs: 58.5% ± 2.4% survival), excluding selective death as underlying reason. DC maturation parameters differed little (Figure 7B). We therefore speculated about distinct antigen handling as an underlying reason and first asked whether medullary DCs were unable to endocytose antigen. However, medullary DCs captured slightly more fluorescent OVA than cortical DCs in an in vitro culture both under homeostatic conditions (Figure 8, A and B) and in NTN (Figure 8B). To test whether medullary DCs might not have antigen access in vivo, we injected fluorescent OVA i.v. into mice and determined its uptake by medullary and cortical DCs. More medullary than cortical DCs captured OVA under homeostatic conditions, and they also took up more filtered antigen per cell (Figure 8, C–E). On day 10 of nephritis, when the mice are heavily proteinuric, the proportion of antigen-containing cortical DCs was as high as that in medullary DCs (Figure 8, C–E). However, the antigen uptake per cell was 3-fold higher in medullary DCs than in cortical DCs (Figure 8, D and E). These findings exclude the possibility that impaired antigen uptake explains the functional defect of medullary DCs.

We next speculated that medullary DCs might function like MPs, which capture more antigen than DCs but degrade it before it can be presented to T cells (41). To test this, we offered the DCs

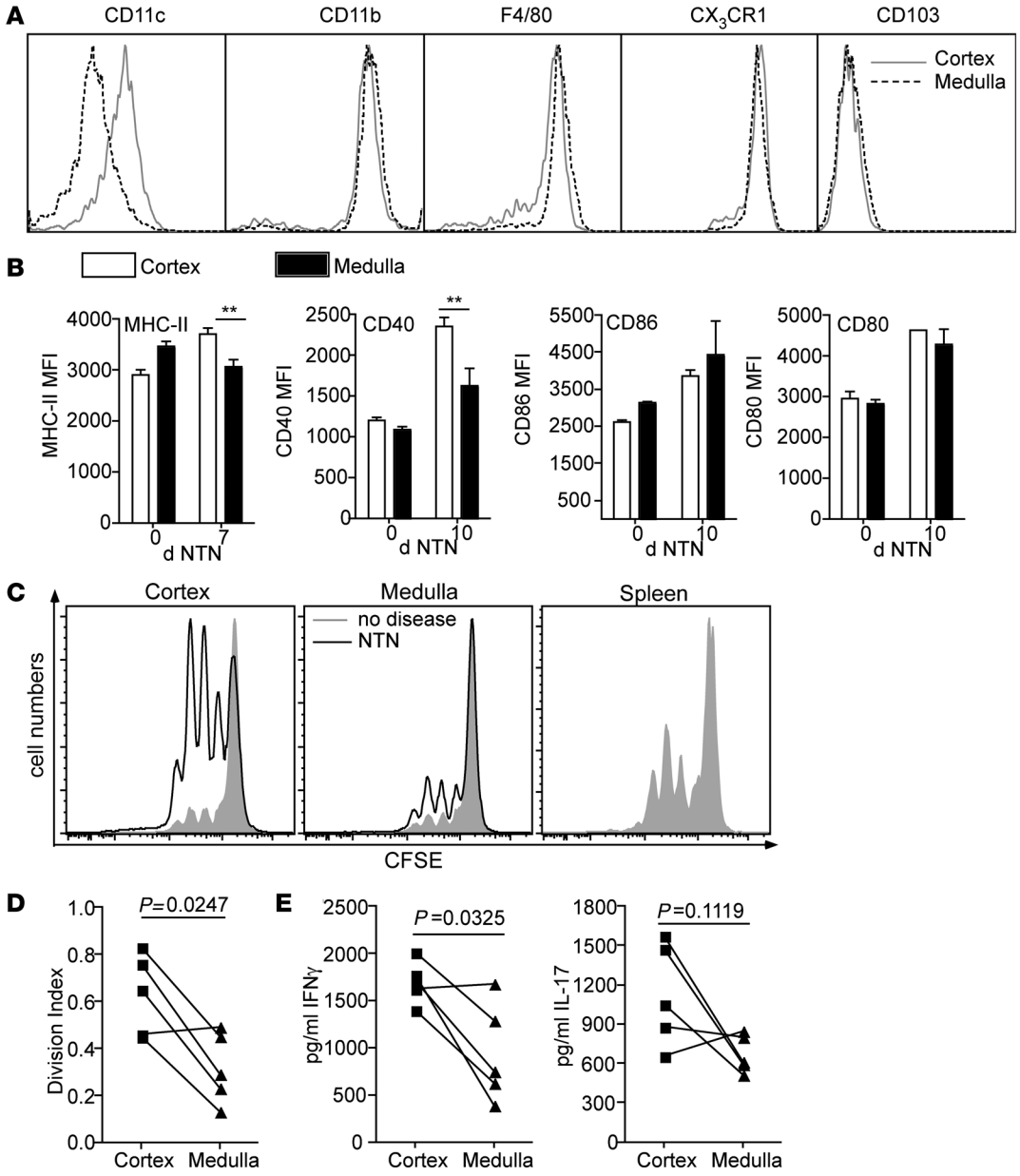

Figure 7

Cortical, but not medullary, DCs can stimulate Th cells in GN. (**A**) Flow cytometric analysis of CX_3CR1^+ APCs from kidney cortices (gray lines) and medullas (black dashed lines) of $CX_3CR1^{GFP/+}$ reporter mice for expression levels of CD11c, CD11b, F4/80, CX_3CR1, and CD103. (**B**) MFI, reflecting expression levels of MHC-II, CD40, CD86, and CD80 on cortical (white bars) and medullary (black bars) DCs in healthy mice (day 0) or mice on day 7 or 10 after NTN induction. (**C**) Representative CFSE dilution profiles, reflecting T cell proliferation in a 72-hour coculture of OVA-specific $CD4^+$ T cells and OVA-loaded cortical, medullary, or splenic DCs derived from healthy (gray solid) or 7-day nephritic (black line) WT mice. 2×10^4 DCs were loaded with 1 mg/ml OVA for 2 hours, washed, and cocultured with 1.5×10^5 OT-II cells for 72 hours. (**D**) Division indices of OT-II cells in coculture from **C**. (**E**) IFN-γ and IL-17 concentrations in 200 μl medium after 72 hours coculture, as in **C**. Results are representative of at least 2 individual experiments, with at least 3 mice per group. Statistical significance was analyzed applying the paired Student's *t* test. $^{**}P < 0.01$.

DQ-OVA, which becomes fluorescent once it is cleaved. Medullary DCs cleaved somewhat more DQ-OVA than cortical DCs (Figure 8F), but this increase correlated with their higher endocytotic activity (Figure 8G). Thus, medullary DCs did not possess the high degradative activity of MPs. This left the explanation that the antigen processing and MHC-II loading machinery is defective in medullary DCs. While the antigen-degrading enzyme cathepsin H was not differentially expressed, there was indeed less expression of invariant chain and H2-DM in medullary DCs, suggesting that medullary DCs are less well equipped to load processed antigen onto MHC-II for presentation to Th cells (Figure 8H).

Medullary DCs regulate innate immunity in the kidney. The inability of medullary DCs to activate Th cells raised the question of what physiological role these cells might play. We reasoned that their

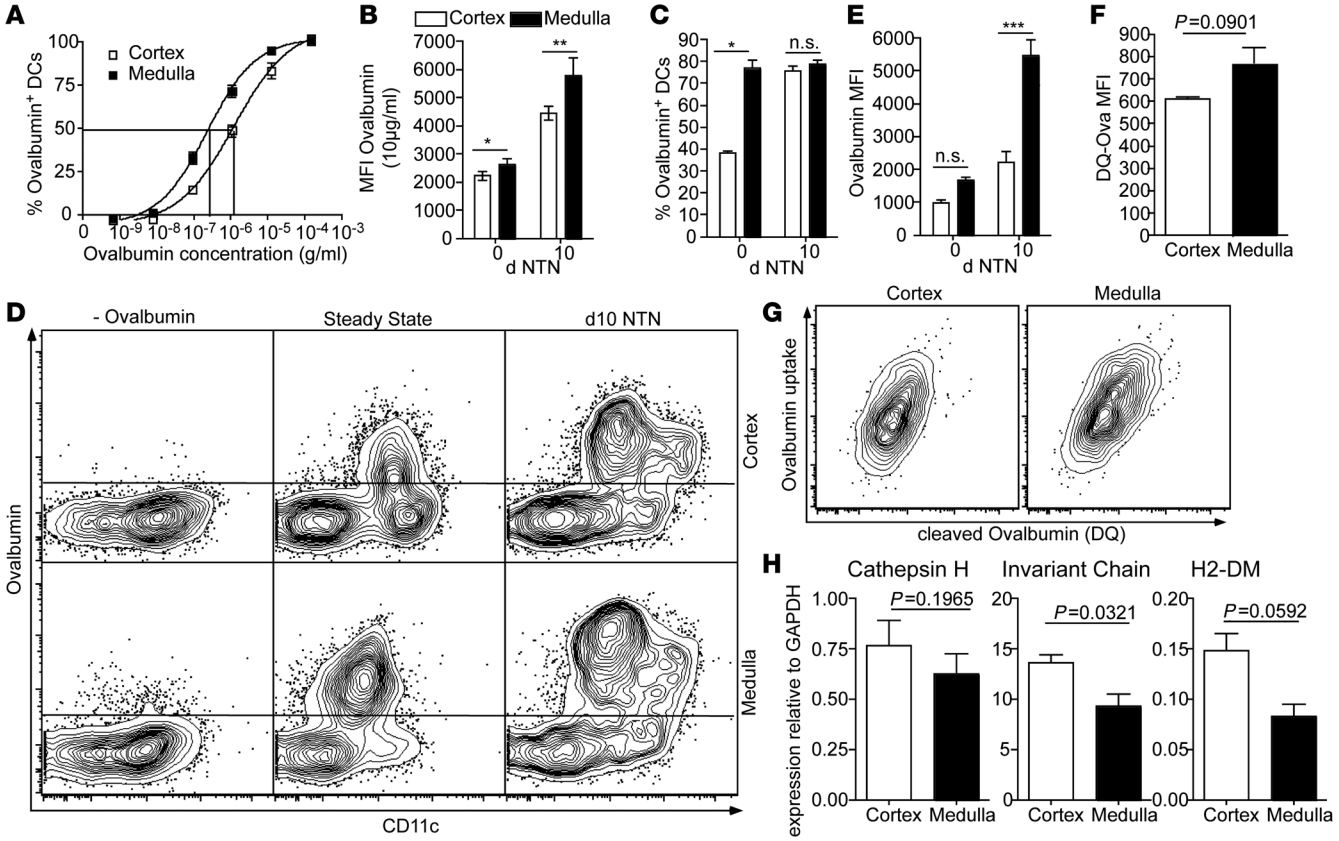

Figure 8

Medullary DCs do not process antigen for MHC-II presentation. (**A**) Uptake of fluorescently labeled OVA by sorted CX_3CR1^+ APCs from kidney cortices (white squares) and medullas (black squares) of healthy $CX_3CR1^{GFP/+}$ reporter mice. Sorted GFP^+ cells were incubated with OVA for 20 minutes at 37°C, washed, and analyzed by flow cytometry. (**B**) Sorted cortical (white bars) and medullary (black bars) DCs from healthy or 10-day nephritic mice were incubated with 10 μg/ml OVA, as in **A**. MFI of OVA^+ cells, reflecting average amount of antigen uptake per cell. (**C**) Percentage of OVA^+ DCs in cortex (white bars) and medulla (black bars) 30 minutes after i.v. injection of fluorescently labeled OVA into healthy or 10-day nephritic mice. (**D**) Representative FACS plots of the in vivo OVA uptake of cortical and medullary $CD45^+MHC\text{-}II^+$ cells in healthy or 10-day nephritic mice, 30 minutes after i.v. injection of Alexa Fluor 647–conjugated OVA. (**E**) MFI of OVA^+ cells in cortex and medulla 30 minutes upon i.v. injection of OVA, as in **C**. (**F**) MFI of cortical and medullary DCs, indicating cleaved DQ-OVA after 20 minutes of incubation with 200 μg/ml DQ-OVA. (**G**) Analysis of cleaved DQ-OVA per endocytosed Alexa Fluor 647–conjugated OVA in cortical and medullary DCs, after 3 hours of incubation with 25 μg/ml DQ-OVA and Alexa Fluor 647–conjugated OVA. (**H**) mRNA for Cathepsin H, invariant chain, and H2-DM in cortical and medullary DCs from 7-day nephritic mice, relative to GAPDH expression. Results represent 2–3 experiments, with 3 to 5 mice per group. Statistical analysis (**B**–**E**) by 1-way ANOVA with Bonferroni test or (**F** and **H**) by paired Student's *t* test. $^*P < 0.05$, $^{**}P < 0.01$, $^{***}P < 0.001$.

location might be particularly suitable for the sentinel function we recently described for kidney DCs in PN (4), because uropathogenic *E. coli* ascend through the collecting ducts in the medulla. To test this hypothesis, we determined DC production of the chemokine CXCL2, which attracts neutrophils into the infected kidney. Indeed, 3 hours after infection, medullary DCs produced far more CXCL2 than cortical DCs (Figure 9, A–C). MPs, identified by lack of CD11c expression, produced very little CXCL2 (Figure 9A).

We next induced PN in CX_3CR1-deficient mice that possess fewer kidney DCs (Figure 1B and Figure 6D) in order to determine consequences for the anti-infectious immune response. Neutrophil numbers in CX_3CR1-deficient mice were somewhat reduced at 3 hours after infection ($CX_3CR1^{+/+}$ mice: $81 \times 10^3 \pm 17 \times 10^3$ neutrophils per kidney; $CX_3CR1^{GFP/GFP}$ mice: $54 \times 10^3 \pm 17 \times 10^3$ neutrophils per kidney; $P < 0.01$), indicating an initial delay of neutrophil recruitment. However, at 6 hours after infection, bacterial CFUs (Figure 9D) and neutrophil numbers (Figure 9E) did not differ between CX_3CR1-deficient and -competent mice. This was not because the fewer DCs in CX_3CR1-deficient mice produced more CXCL2 per cell ($CX_3CR1^{GFP/+}$ mice: $MFI_{CXCL2} = 7{,}957 \pm 774$; $CX_3CR1^{GFP/GFP}$ mice: $MFI_{CXCL2} = 7{,}948 \pm 487$). Instead, we found that neutrophils commenced robust CXCL2 production at 6 hours after infection (Figure 9F). This suggested that the medullary DCs in CX_3CR1-deficient mice were sufficient for initiating neutrophil recruitment, and once neutrophils were present in the infected kidney, they produced large amounts of CXCL2. This production compensated for the DC deficiency in the absence of CX_3CR1 with respect to antibacterial immune defense.

Discussion

CX_3CR1 is widely used to identify APCs in various tissues, but few functional roles have been described. Here we report that CX_3CR1 strongly affects the abundance of DCs, but not of MPs, in the kidney. The small intestine was the only other organ demon-

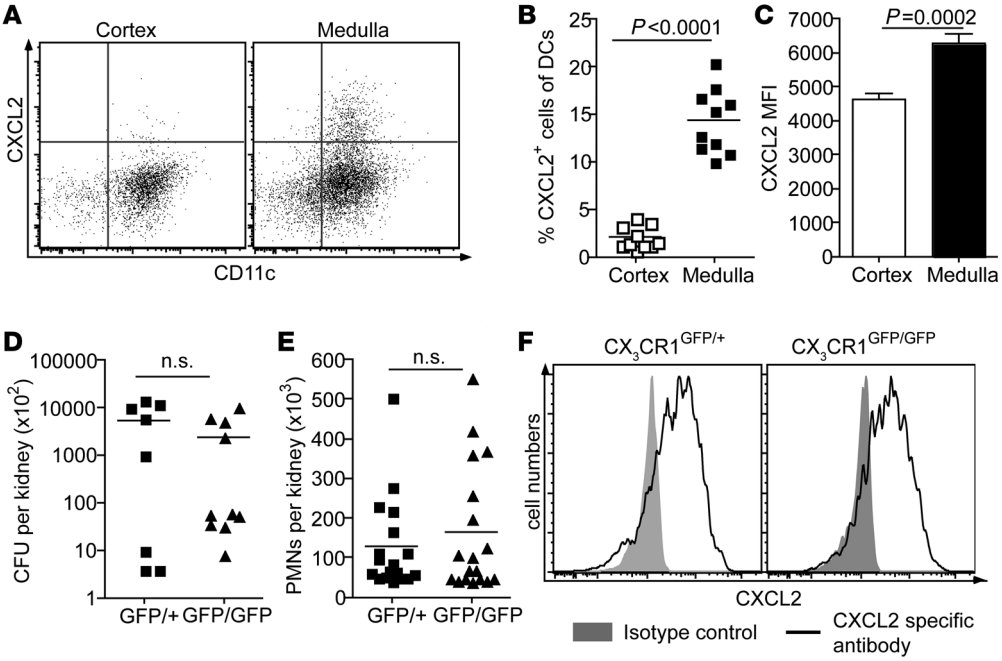

Figure 9

Medullary DCs regulate the innate immunity against PN. (**A**) Representative FACS plots of CXCL2 production by CD45$^+$MHC-II$^+$ cells in kidney cortex and medulla 3 hours after second UPEC instillation. Cells were incubated with brefeldin A for 4 hours at 37°C prior to staining. (**B**) Percentage of CXCL2-producing cells of CD45$^+$MHC-II$^+$CD11c$^+$ cells in cortex (white squares) and medulla (black squares). (**C**) MFI for CXCL2 of cortical and medullary CXCL2$^+$ DCs, representing CXCL2 production per cell. (**D**) CFUs per kidney in $CX_3CR1^{GFP/+}$ reporter mice and $CX_3CR1^{GFP/GFP}$-deficient mice 6 hours after second UPEC instillation. (**E**) Numbers of neutrophils (PMNs) per kidney in $CX_3CR1^{GFP/+}$ and $CX_3CR1^{GFP/GFP}$ mice 6 hours after second UPEC instillation. (**F**) Representative histogram of CXCL2 staining (black line) of CD45$^+$Ly6G$^+$ neutrophils from $CX_3CR1^{GFP/+}$ and $CX_3CR1^{GFP/GFP}$ mice 6 hours after second UPEC instillation, compared with isotype control (gray solid). Cells were incubated with brefeldin A for 4 hours at 37°C prior to staining. Data points represent individual mice; and results are representative of 2 to 3 individual experiments, with 6 mice per group. Statistical significance was analyzed by (**B** and **C**) Wilcoxon signed-rank test or (**D** and **E**) 2-tailed Mann-Whitney nonparametric test.

strating APC dependence on CX_3CR1 under homeostatic conditions, albeit primarily affecting MPs. The kidney and the intestine expressed the highest levels of CX_3CL1 of all organs tested, providing a plausible explanation for the CX_3CR1 dependency of kidney DCs. This identifies CX_3CR1 as a chemokine receptor that targets kidney DCs with relative specificity. To our knowledge, this is the first example of an organ-specific chemokine receptor that affects DCs rather than lymphocytes.

The CX_3CR1 dependence of kidney DCs in the steady state may theoretically result from an effect on precursor recruitment, their differentiation into DCs, or on DC survival/retention in the kidney. The slow turnover of kidney DCs in the steady state (42) hinders discriminating among these possibilities. Under inflammatory conditions, recruitment of DC precursors to the kidney partially depended on this CX_3CR1. This is consistent with previous studies showing CX_3CR1-dependent monocyte recruitment and/or survival to inflamed vessels and liver (29–31). CX_3CR1^+ monocytes can give rise to both DCs and MPs (5, 33). However, we have not formally shown that monocytes were the precursors of DCs in NTN. This may be doable by using CCR2-deficient mice, in which inflammatory monocytes cannot leave the bone marrow (43). Furthermore, it remained unclear why CX_3CR1 selectively affected DCs, but not MPs, in homeostasis, although both cell types express this receptor. Further studies may clarify the exact ontogeny of kidney DCs in homeostasis and inflammation (44, 45).

Kidney DC numbers were reduced also in nephritic CX_3CR1-deficient mice. Consequently, intrarenal DC-dependent inflammation and the course of crescentic GN were markedly attenuated in CX_3CR1-deficient mice. This confirmed our previous study, in which we observed NTN attenuation after depleting kidney DCs with the use of CD11c-DTR mice (13). However, in that study, we unavoidably depleted DCs also in other tissues, which may be functionally relevant. Furthermore, CD11c-DTR mice are hampered by a side effect, bone marrow release of neutrophils and monocytes after DC depletion, which can impact immune responses, especially in PN (46). Our present findings allow conclusions regarding kidney DCs in the absence of these shortcomings. Furthermore, they suggest that targeting CX_3CR1 might be useful for treating GN, especially since not only DCs, but also MPs (the DTH effector cells), were to some extent CX_3CR1 dependent in kidney inflammation.

The particularly strong CX_3CR1 dependence of cortical DCs and their intrarenal location suggested that NTN is primarily driven by these DCs. Indeed, only cortical DCs were able to activate Th cells. This activation is important in NTN, because it induces chemokines and cytokines that assemble and maintain the tubulointerstitial infiltrates that drive disease progression (2, 11, 13). Mechanistic analysis revealed that the inability of medullary DCs to activate T cells did neither result from their failure to mature, nor from defective antigen uptake. On the con-

trary, medullary DCs were superior at endocytosis, despite being "downstream" of the nephron from cortical DCs and thus further away from antigen filtered under proteinuric conditions. Instead, our findings support the interpretation that only cortical DCs processed the antigen they captured in a manner suitable to stimulate Th cells. These findings demonstrate that cortical and medullary DC functions differ.

The inability of medullary DCs to perform the hallmark DC function, activating T cells, raised the question of whether these cells can still be considered DCs. Some recent studies on intestinal APCs proposed that $CD11c^+CX_3CR1^+$ cells should be generally considered MPs and that only $CD103^+CD11c^+$ phagocytes represent DCs (22, 47, 48), but this is not generally accepted (49). In contrast to the intestine, almost all DCs in the kidney are $CX_3CR1^+CD11c^+$, whereas $CD103^+$ DCs are a minority of less than 5% (50). We had previously classified $CD11c^+$ kidney APCs as DCs, because they resembled splenic DCs in their ability to activate T cells (6). Also their transcriptome is closer to that of tissue DCs than that of MPs (7). These findings did not exclude that only a subset of kidney $CD11c^+$ cells was capable of T cell activation, and here we show that only cortical $CD11c^+$ cells did so, at least in NTN. We speculated that medullary $CD11c^+$ cells might functionally resemble MPs, given that they captured large amounts of antigen in vivo. However, this was most likely due to the concentration of filtered antigen in the kidney medulla, which exposed cells in this compartment to higher antigen quantities. The in vitro antigen uptake of medullary DCs was only somewhat higher than that of cortical DCs. Moreover, medullary DCs did not degrade antigen too swiftly for antigen presentation, which has been stated to be characteristic of MPs (41). Instead, we found that medullary DCs were specialized at sentineling against PN. For this purpose, these DCs are strategically positioned adjacent to the collecting ducts through which UPECs first pass when they invade the kidney. In response to infection, medullary DCs rapidly produced neutrophil-attracting chemokines like CXCL2. Cortical DCs produced fewer chemokines, and MPs produced none, at least at the early time points that we examined. This sentinel function appears more compatible with the regulatory role of DCs, rather than with the immune effector functions of MPs. However, there is far more plasticity between these cell types than previously thought, especially in the kidney (51). Final classification of these APCs requires more discussion and a general consensus. For clarity, we will continue to refer to medullary $CD11c^+$ APCs as DCs.

The defense against PN was barely impaired in CX_3CR1-deficient mice, whereas DC depletion with the use of CD11c-DTR mice had delayed this defense (4). These transgenic mice usually achieve higher kidney DC depletion rates than those observed for medullary DCs in CX_3CR1-deficient mice. The remaining medullary DCs apparently sufficed to initiate neutrophil recruitment. This recruitment was somewhat less efficient, but once the first neutrophils had entered, they produced CXCL2 themselves and the bacteria were cleared with little delay. This can only operate in infections, in which delayed immune cell recruitment aggravates disease, but not in immune-mediated diseases, in which such a delay would be protective. Compensatory chemokine production by neutrophils, together with the minor effect of CX_3CR1 on medullary DCs, can explain why the lack of this receptor only marginally affected PN.

In conclusion, we have shown that cortical and medullary DCs are specialized at regulating adaptive and innate immune responses in NTN and PN, respectively. The abundance of cortical, and to a lesser extent of medullary DCs, depended on CX_3CR1 expression. The relative kidney specificity of this receptor recommends it as a potential therapeutic target in immune-mediated kidney diseases, especially as the susceptibility to bacterial infections was not markedly increased. Thus, targeting CX_3CR1, for example, by systemic injection of blocking antibodies or recombinant CX_3CL1 (21, 37), might represent a promising treatment for GN with fewer side effects than general immunosuppressive therapies. Future studies are required to assess the benefit of CX_3CR1-mediated DC targeting in the kidney compared with potential side effects resulting from the loss of other CX_3CR1 functions.

Methods

Animals. C57/BL6 mice, $CX_3CR1^{GFP/+}$ reporter mice, and $CX_3CR1^{GFP/GFP}$-deficient mice were bred and kept in specific pathogen–free conditions at the animal facility of the University of Bonn. All lines had been backcrossed more than 10 times onto the C57BL/6 background.

Isolation of murine kidney DCs and OT-II cells. Complete kidneys or cortex and medulla preparations were digested with collagenase (Roche Diagnostic) and DNAse-I, as previously described (6). Tubular fragments from digested kidneys were removed by filtration. $CD11c^+$ DCs were then enriched using nanobead-labeled CD11c-specific monoclonal antibodies (clone N418) (Miltenyi). Magnetic bead separation was carried out according to manufacturer's instructions. Purity was typically 90%–95% of $CD45^+$ cells. OT-II cells were isolated from spleens and lymph nodes of OT-II mice and enriched using a commercially available $CD4^+$ T Cell Isolation Kit (Miltenyi). Purity was usually about 85% of $CD45^+$ cells.

Flow cytometry. After treatment with Fc-blocking antibodies (clone 2.4G2), cells were stained for 15 minutes on ice with fluorochrome-labeled monoclonal antibodies against CD11c (clone HL3), I-Ab (AF6-120.1), and CD40 (3/23) (BD Biosciences) as well as CD45 (30-F11), CD11b (M1/70), Gr1 (RB6-8C5), CD4 (GK1.5), CD3 (145-2C11), CD86 (GL1), CD80 (16-10A1), and CD103 (2E7) (eBioscience). For intracellular cytokine staining, single cell suspensions were incubated in RPMI (10% FCS) with 1 μl/ml GolgiPlug and 1 μl/ml GolgiStop (BD Biosciences) for 4 hours at 37°C. T cells were restimulated with PMA/ionomycin for 4.5 hours, starting 30 minutes before addition of GolgiPlug and GolgiStop. After cell surface staining, cells were fixated in 4% formalin (Morphisto GmbH) for 10 minutes on ice. Cell membranes were permeabilized with PermWash (BD Biosciences) for 15 minutes at room temperature. Intracellular staining was performed in PermWash for 20 minutes at room temperature using flourochrome-labeled monoclonal antibodies against TNF-α (clone MP6-XT22), IFN-γ (XMG1.2), and IL-17 (9D3.1C8). Cells were analyzed with a BDCantoII (Becton Dickinson).

T cell activation assays. Either mice were injected with 1 mg OVA 1 hour prior to harvesting kidneys or isolated cortical and medullary DCs were loaded in vitro for 2 hours with 1 mg/ml OVA. DCs were cocultured with OT-II cells in 200 μl RPMI (10% FCS) in 96-well plates for 72 hours. T cell proliferation was measured by CFSE dilution. Therefore, isolated T cells were stained with 1 nM CFSE in PBS for 10 minutes at 37°C and washed twice with ice-cold RPMI (10% FCS). Cytokine induction was analyzed by intracellular staining of OT-II cells for IFN-γ and IL-17. Cytokines in the supernatants were measured using the Th1/Th2 10plex FlowCytomix Multiplex Kit (Bender MedSystems).

Endocytosis and cleavage assays. For comparing the uptake of filterable antigen by cortical and medullary DCs in vivo, mice were injected with 500 ng Alexa Fluor 647–conjugated OVA (Invitrogen) per g body weight. Single cell suspensions were obtained from kidney cortices and medullas 30 minutes after antigen injection. Cells were stained and analyzed via flow cytometry. For in vitro uptake studies, cortical and medullary

DCs were sorted with a FACSDiva (Becton Dickinson). Cells were then incubated with indicated OVA concentrations for 30 minutes at 37°C, washed, and analyzed by flow cytometry. For comparing the antigen cleavage, DQ-OVA (Invitrogen), which becomes fluorescent upon cleavage, was used in addition to Alexa Fluor 647–conjugated OVA, which served as a control for antigen uptake.

RNA preparation and RT-PCR. RNA from FACS-sorted cortical and medullary DCs was extracted using TRIzol (Invitrogen) and Chlorophorm (Carl Roth) according to standard laboratory methods. Whole tissue RNA was extracted using the RNA NucleoSpin Kit (Macherey-Nagel) according to manufacturer's instructions. RNA was reverse transcribed into cDNA using the High-Capacity Reverse Transcription Kit (Applied Biosystems). Quantitative PCR was performed for 40 cycles using SYBR Green (Applied Biosystems). The following primer sequences were used: invariant chain (forward) 5′-AGGCTCCACCTAAAGAGCCACTG-3′, (reverse) 5′-ACAGACACCAGTCTCAAGCCCC-3′; H2-DM (forward) 5′-ACGTGCGTGCTGAATGATGCT-3′, (reverse) 5′-AGCCCGTTTTGCAAGCGATGAATA-3′; cathepsin H (forward) 5′-AACATGTGTGGCCTGGCTGC-3′, (reverse) 5′-TGATGTCACGTGGGTGGGCT-3′; and CX3CL1 (forward) 5′-GCCGCGTTCTTCCATTTG-3′, (reverse) 5′-CGCACATGATTTCGCATTTC-3′. All samples were run in triplicate and normalized to GAPDH or 18s rRNA.

Induction of NTN and functional studies. Nephrotoxic serum nephritis was induced in 8- to 12-week-old age- and sex-matched CX_3CR1 reporter, CX_3CR1-deficient, and WT mice by i.v. injection of a cumulative dose of 13 μl per g bodyweight on 3 consecutive days or by i.p. injection of 0.5 ml NTN serum per mouse, as previously described (13, 52). On day 4 and 9, urine was collected in metabolic cages for 12 hours. Mice were culled on day 10 or on day 15. Flow cytometrical analysis and analysis of creatinine clearance were performed on day 10 after disease induction. Histological analysis was performed on day 15. Serum was derived from whole blood after cardiac puncture. Urinary creatinine and serum creatinine were measured using standard laboratory methods in the Central Laboratory of the University Hospital of Bonn. Creatinine clearance was calculated by the formula $C_{Cr} = (U_{Cr} \times Vol_U)/(S_{Cr} \times t)$, where C_{Cr} stands for creatinine clearance, U_{Cr} stands for creatinine concentration in urine, Vol_U stands for urine volume (in ml), S_{Cr} stands for creatinine concentration in serum, and t stands for time in metabolic cage (in minutes).

Transfer experiments. Total bone marrow cells were obtained from the femurs of CX_3CR1 reporter and CX_3CR1-deficient mice. 10^7 bone marrow cells, of which approximately 10% expressed GFP, were transferred into WT mice, which had been injected with nephrotoxic sheep serum (NTS) 1 day before. Single cell suspensions were obtained after 48 or 96 hours from kidneys and spleens. Proportions of GFP^+ cells among $CD45^+$ cells and phenotype of these cells were determined by flow cytometry.

Histology. Fluorescence microscopy was performed on 3-μm paraffin sections in PFA-fixed kidneys derived from healthy and 10-day nephritic $CX_3CR1^{GFP/+}$ reporter mice and $CX_3CR1^{GFP/GFP}$-deficient mice. GFP^+ cells were quantified using CellF software (Olympus). Light microscopy was performed on 3-μm paraffin sections of PFA-fixed tissue derived from 15-day nephritic mice, stained by Masson's trichrome coloration using standard protocols. Kidney damage was histologically scored by an observer blinded to the identity of samples. For determining the proportion of crescentic glomeruli, at least 80 glomeruli per section were examined. $F4/80^+$ cells were stained using rabbit antibody to F4/80 (MCA497B, Serotec) diluted 1:50. $F4/80^+$ cell infiltration was then quantified using ImageJ software (NIH).

Urinary tract infection model. Uropathogenic *E. coli* strain 536 (UPEC) (53) were grown for 5 hours at 37 °C in LB medium. Bacteria were harvested by centrifugation at 1,200 *g* for 10 minutes and resuspended in 2 ml LB medium to a final concentration of 1×10^{10} CFUs per ml. Female mice of 8 to 12 weeks of age were anesthetized with Avertin (40 mg 2,2,2-tri bromoethanol, Sigma-Aldrich) dissolved in 1 ml tert-amyl alcohol (0.01 ml g^{-1} body weight i.p.) and were infected by transurethral instillation of 1×10^9 UPEC using a flexible polyethylene catheter (outer diameter 0.6 mm; BD) coated with Instillagel (Farco Pharma). Three hours later the procedure was repeated to induce PN. Before analysis, mice were perfused with sterile PBS. The number of ascended bacteria was quantified by scoring CFUs after overnight culture of kidney collagenase digest or by homogenization in PBS with an Ultra Turrax at 37°C on CPS ID plates (Biomerieux), as described previously.

Statistics. Results are expressed as mean ± SEM. Comparisons were drawn using a 2-tailed paired Student's *t* test or the nonparametric Wilcoxon signed-rank test (cortex and medulla from 1 mouse) or unpaired Student's *t* test, 1-way ANOVA in combination with Bonferroni multiple-comparison test, or the 2-sided nonparametric Mann Whitney *U* test (comparison between individual mice) (Prism 4, Graphpad Software). *P* values of less than 0.05 were considered significant.

Study approval. All animal studies have been approved by The Landesamt für Natur, Umwelt und Verbraucherschutz Nordrhein Westfalen, Recklinghausen, Germany.

Acknowledgments

The authors thank Steffen Jung for CX_3CR1-knockin mice; Anke Carstensen for the analysis of mouse serum and urine; Anett Peters, Chrystel Llanto, and Jessica Gonyer for technical assistance; and Bart Lambrecht and Natalio Garbi for helpful suggestions. We acknowledge support by the Central Animal Facilities and the Flow Cytometry Core Facility of the Medical Faculty of Bonn University. K. Hochheiser is supported by a fellowship of the German National Academic Foundation (Studienstiftung des Deutschen Volkes). This work was supported by the Deutsche Forschungsgemeinschaft (KFO228, SFB704, SFBTR57, Leibniz award to C. Kurts). P.A. Knolle and C. Kurts are members of the Excellence Cluster "Immunosensation."

Received for publication March 26, 2013, and accepted in revised form July 3, 2013.

Address correspondence to: Katharina Hochheiser, Institutes of Molecular Medicine and Experimental Immunology (IMMEI), Friedrich-Wilhelms-Universität, 53105 Bonn, Germany. Phone: 49.228.287.11033; Fax: 49.228.287.11052; E-mail: khochhei@uni-bonn.de. Or to: Christian Kurts, Institutes of Molecular Medicine and Experimental Immunology (IMMEI), Friedrich-Wilhelms-Universität, 53105 Bonn, Germany. Phone: 49.228.287.11050; Fax: 49.228.287.11052; E-mail: ckurts@web.de.

1. Wakim LM, Waithman J, van Rooijen N, Heath WR, Carbone FR. Dendritic cell-induced memory T cell activation in nonlymphoid tissues. *Science*. 2008;319(5860):198–202.
2. Heymann F, et al. Kidney dendritic cell activation is required for progression of renal disease in a mouse model of glomerular injury. *J Clin Invest*. 2009;119(5):1286–1297.
3. Riedel JH, et al. Immature renal dendritic cells recruit regulatory CXCR6(+) invariant natural killer T cells to attenuate crescentic GN. *J Am Soc Nephrol*. 2012;23(12):1987–2000.
4. Tittel AP, Heuser C, Ohliger C, Knolle PA, Engel DR, Kurts C. Kidney dendritic cells induce innate immunity against bacterial pyelonephritis. *J Am Soc Nephrol*. 2011;22(8):1435–1441.
5. Geissmann F, Manz MG, Jung S, Sieweke MH, Merad M, Ley K. Development of monocytes, macrophages, and dendritic cells. *Science*. 2010; 327(5966):656–661.
6. Kruger T, et al. Identification and functional characterization of dendritic cells in the healthy murine kidney and in experimental glomerulonephritis. *J Am Soc Nephrol*. 2004;15(3):613–621.

7. Miller JC, et al. Deciphering the transcriptional network of the dendritic cell lineage. *Nat Immunol*. 2012;13(9):888–899.
8. Soos TJ, et al. CX3CR1+ interstitial dendritic cells form a contiguous network throughout the entire kidney. *Kidney Int*. 2006;70(3):591–596.
9. Dong X, Swaminathan S, Bachman LA, Croatt AJ, Nath KA, Griffin MD. Resident dendritic cells are the predominant TNF-secreting cell in early renal ischemia-reperfusion injury. *Kidney Int*. 2007;71(7):619–628.
10. Dong X, Bachman LA, Miller MN, Nath KA, Griffin MD. Dendritic cells facilitate accumulation of IL-17 T cells in the kidney following acute renal obstruction. *Kidney Int*. 2008;74(10):1294–1309.
11. Tipping PG, Holdsworth SR. T cells in crescentic glomerulonephritis. *J Am Soc Nephrol*. 2006; 17(5):1253–1263.
12. Scholz J, et al. Renal dendritic cells stimulate IL-10 production and attenuate nephrotoxic nephritis. *J Am Soc Nephrol*. 2008;19(3):527–537.
13. Hochheiser K, et al. Kidney dendritic cells become pathogenic during crescentic glomerulonephritis with proteinuria. *J Am Soc Nephrol*. 2011;22(2):306–316.
14. Paust HJ, et al. Chemokines play a critical role in the cross-regulation of Th1 and Th17 immune responses in murine crescentic glomerulonephritis. *Kidney Int*. 2012;82(1):72–83.
15. Mora JR, et al. Selective imprinting of gut-homing T cells by Peyer's patch dendritic cells. *Nature*. 2003;424(6944):88–93.
16. Campbell JJ, et al. The chemokine receptor CCR4 in vascular recognition by cutaneous but not intestinal memory T cells. *Nature*. 1999;400(6746):776–780.
17. Panina-Bordignon P, et al. The C-C chemokine receptors CCR4 and CCR8 identify airway T cells of allergen-challenged atopic asthmatics. *J Clin Invest*. 2001;107(11):1357–1364.
18. Reboldi A, et al. C-C chemokine receptor 6-regulated entry of TH-17 cells into the CNS through the choroid plexus is required for the initiation of EAE. *Nat Immunol*. 2009;10(5):514–523.
19. Villares R, et al. CCR6 regulates EAE pathogenesis by controlling regulatory CD4+ T-cell recruitment to target tissues. *Eur J Immunol*. 2009;39(6):1671–1681.
20. Jung S, et al. Analysis of fractalkine receptor CX(3) CR1 function by targeted deletion and green fluorescent protein reporter gene insertion. *Mol Cell Biol*. 2000;20(11):4106–4114.
21. Lee YS, et al. The fractalkine/CX3CR1 system regulates β cell function and insulin secretion. *Cell*. 2013;153(2):413–425.
22. Medina-Contreras O, et al. CX3CR1 regulates intestinal macrophage homeostasis, bacterial translocation, and colitogenic Th17 responses in mice. *J Clin Invest*. 2011;121(12):4787–4795.
23. Niess JH, et al. CX3CR1-mediated dendritic cell access to the intestinal lumen and bacterial clearance. *Science*. 2005;307(5707):254–258.
24. Kim KW, et al. In vivo structure/function and expression analysis of the CX3C chemokine fractalkine. *Blood*. 2011;118(22):e156–e167.
25. Cockwell P, Calderwood JW, Brooks CJ, Chakravorty SJ, Savage CO. Chemoattraction of T cells expressing CCR5, CXCR3 and CX3CR1 by proximal tubular epithelial cell chemokines. *Nephrol Dial Transplant*. 2002;17(5):734–744.
26. Segerer S, Hughes E, Hudkins KL, Mack M, Goodpaster T, Alpers CE. Expression of the fractalkine receptor (CX3CR1) in human kidney diseases. *Kidney Int*. 2002;62(2):488–495.
27. Hoffmann U, et al. Impact of chemokine receptor CX3CR1 in human renal allograft rejection. *Transpl Immunol*. 2010;23(4):204–208.
28. Haskell CA, et al. Targeted deletion of CX(3)CR1 reveals a role for fractalkine in cardiac allograft rejection. *J Clin Invest*. 2001;108(5):679–688.
29. Tacke F, et al. Monocyte subsets differentially employ CCR2, CCR5, and CX3CR1 to accumulate within atherosclerotic plaques. *J Clin Invest*. 2007;117(1):185–194.
30. Landsman L, et al. CX3CR1 is required for monocyte homeostasis and atherogenesis by promoting cell survival. *Blood*. 2009;113(4):963–972.
31. Karlmark KR, et al. The fractalkine receptor CX(3) CR1 protects against liver fibrosis by controlling differentiation and survival of infiltrating hepatic monocytes. *Hepatology*. 2010;52(5):1769–1782.
32. Combadiere C, et al. CX3CR1-dependent subretinal microglia cell accumulation is associated with cardinal features of age-related macular degeneration. *J Clin Invest*. 2007;117(10):2920–2928.
33. Auffray C, et al. CX3CR1+ CD115+ CD135+ common macrophage/DC precursors and the role of CX3CR1 in their response to inflammation. *J Exp Med*. 2009;206(3):595–606.
34. Li L, et al. The chemokine receptors CCR2 and CX3CR1 mediate monocyte/macrophage trafficking in kidney ischemia-reperfusion injury. *Kidney Int*. 2008;74(12):1526–1537.
35. Furuichi K, Gao JL, Murphy PM. Chemokine receptor CX3CR1 regulates renal interstitial fibrosis after ischemia-reperfusion injury. *Am J Pathol*. 2006;169(2):372–387.
36. Shimizu K, et al. Fractalkine and its receptor, CX3CR1, promote hypertensive interstitial fibrosis in the kidney. *Hypertens Res*. 2011;34(6):747–752.
37. Feng L, et al. Prevention of crescentic glomerulonephritis by immunoneutralization of the fractalkine receptor CX3CR1 rapid communication. *Kidney Int*. 1999;56(2):612–620.
38. Plantinga M, et al. Conventional and monocyte-derived CD11b(+) dendritic cells initiate and maintain T helper 2 cell-mediated immunity to house dust mite allergen. *Immunity*. 2013;38(2):322–335.
39. Kurts C, Heymann F, Lukacs-Kornek V, Boor P, Floege J. Role of T cells and dendritic cells in glomerular immunopathology. *Semin Immunopathol*. 2007;29(4):317–335.
40. Lukacs-Kornek V, Burgdorf S, Diehl L, Specht S, Kornek M, Kurts C. The kidney-renal lymph node-system contributes to cross-tolerance against innocuous circulating antigen. *J Immunol*. 2008;180(2):706–715.
41. Delamarre L, Pack M, Chang H, Mellman I, Trombetta ES. Differential lysosomal proteolysis in antigen-presenting cells determines antigen fate. *Science*. 2005;307(5715):1630–1634.
42. Dong X, Swaminathan S, Bachman LA, Croatt AJ, Nath KA, Griffin MD. Antigen presentation by dendritic cells in renal lymph nodes is linked to systemic and local injury to the kidney. *Kidney Int*. 2005;68(3):1096–1108.
43. Serbina NV, Pamer EG. Monocyte emigration from bone marrow during bacterial infection requires signals mediated by chemokine receptor CCR2. *Nat Immunol*. 2006;7(3):311–317.
44. Shortman K, Naik SH. Steady-state and inflammatory dendritic-cell development. *Nat Rev Immunol*. 2007;7(1):19–30.
45. Liu K, et al. In vivo analysis of dendritic cell development and homeostasis. *Science*. 2009;324(5925):392–397.
46. Tittel AP, et al. Functionally relevant neutrophilia in CD11c diphtheria toxin receptor transgenic mice. *Nat Methods*. 2012;9(4):385–390.
47. Schulz O, et al. Intestinal CD103+, but not CX3CR1+, antigen sampling cells migrate in lymph and serve classical dendritic cell functions. *J Exp Med*. 2009;206(13):3101–3114.
48. Zigmond E, et al. Ly6C hi monocytes in the inflamed colon give rise to proinflammatory effector cells and migratory antigen-presenting cells. *Immunity*. 2012;37(6):1076–1090.
49. Bogunovic M, et al. Origin of the lamina propria dendritic cell network. *Immunity*. 2009;31(3):513–525.
50. Ginhoux F, et al. The origin and development of nonlymphoid tissue CD103+ DCs. *J Exp Med*. 2009;206(13):3115–3130.
51. Nelson PJ, Rees AJ, Griffin MD, Hughes J, Kurts C, Duffield J. The renal mononuclear phagocytic system. *J Am Soc Nephrol*. 2012;23(2):194–203.
52. Bollee G, et al. Epidermal growth factor receptor promotes glomerular injury and renal failure in rapidly progressive crescentic glomerulonephritis. *Nat Med*. 2011;17(10):1242–1250.
53. Godaly G, Proudfoot AE, Offord RE, Svanborg C, Agace WW. Role of epithelial interleukin-8 (IL-8) and neutrophil IL-8 receptor A in Escherichia coli-induced transuroepithelial neutrophil migration. *Infect Immun*. 1997;65(8):3451–3456.